Pergamon

PII: S1359-6454(96)00323-0

Acta mater. Vol. 45, No. 5, pp. 1907–1915, 1997

1359-6454/97 $17.00 + 0.00

A FINITE ELEMENT METHOD FOR SIMULATING INTERFACE MOTION—I. MIGRATION OF PHASE AND GRAIN BOUNDARIES

B. SUN[1,†], Z. SUO[1,‡] and W. YANG[2]

[1]Mechanical and Environmental Engineering Department, and Materials Department, University of California, Santa Barbara, CA 93106, U.S.A. and [2]Engineering Mechanics Department, Tsinghua University, Beijing 100084, P.R. China

(Received 22 April 1996; accepted 26 August 1996)

Abstract—This paper describes a finite element method for simulating migration of interfaces (e.g. phase and grain boundaries) in materials. The method is built on a classical theory. Each individual grain is in an equilibrium state; interface tension and bulk phase chemical potential constitute the free energy. An interface migrates—as atoms break from one grain, cross the interface, and attach to the other grain—at a velocity proportional to the free energy reduction per unit volume of atoms crossing the interface. We express this theory in a weak statement, model the interfaces with finite elements, and update nodal positions incrementally. The variations of the free energy, associated with the virtual motions of the nodes, define the generalized forces. The weak statement connects the generalized forces and the nodal velocities with a viscosity matrix. The method takes into account large interface shape changes, interface tension anisotropy, and non-equilibrium triple junctions (if present). We illustrate the method with examples including grooving on a polycrystal surface, grain growth in a thin film, and facet formation of a single crystal particle. © *1997 Acta Metallurgica Inc.*

1. INTRODUCTION

Interface motion plays a decisive role in many material technologies. During ceramic sintering, for example, pores and grains co-evolve: pores shrink, grains grow, and pores move with, or detach from, grain boundaries. Properties (e.g. strength and transparency) of an end product depend on the size and distribution of the pores and grains [1, 2]. Another example involves polycrystalline thin films. A thermal anneal may cause a thin film to evolve along different paths, ranging from substantial grain growth to island formation [3, 4].

In either example, the material selects its morphology by a dynamical process, rather than an equilibrium state. The structural changes result from a complex interplay of multiple forces and concomitant processes. They are regulated by time, temperature, pressure, impurities and vapor environment. It is this complexity that enables the control and improvement of industrial processes. The complexity also calls for theoretical simulations to map out diverse evolution paths and identify regulatory parameters. This paper and its sequel describe a finite element approach to simulating interface motions under various conditions.

Surface tension is a significant force that drives structural evolution at small length scales. Herring [5] examined the variation of total surface energy per unit volume of atoms added on a surface, and paid particular attention to surface tension that varies with crystalline orientation and causes facets. Turnbull [6] described a theory of interface migration controlled phase change, where each phase is in an equilibrium state, and the interface velocity is set by the process of atoms breaking from one phase and attaching to the other. The interface velocity relates to the free energy reduction per unit volume of atoms crossing the interface. The theory has been adopted in modeling, e.g. evaporation–condensation [7], grain growth [8, 9], and shape changes of faceted crystals [10].

This interface migration theory has an equivalent variational statement [11]. It has been used to study shape instability of a pore in an elastic crystal [11], and domain evolution in a ferroelectric crystal [12]. Finite element methods have been formulated on the basis of the variational statement to simulate grain growth [13, 14]. The present paper builds on these ideas and describes a finite element program to simulate a larger class of physical processes by including surface tension anisotropy, bulk phase free energy density, and finite junction mobility.

2. BASIC THEORY AND ITS WEAK STATEMENT

Consider a system of interfaces separating a vapor phase, solid phases and grains. We make the

†Present address: Applied Magnetics Corporation, 75 Robin Hill Road, Coleta, CA 93117, U.S.A.
‡To whom all correspondence should be addressed.

following assumptions of the vapor. Atoms diffuse so fast in the vapor relative to the rate of interface reaction that the vapor has a spatially uniform chemical potential. The amount of vapor is so large compared to the mass exchange due to evaporation and condensation that the vapor keeps its chemical potential constant at all times. Thus, the solid is in contact with an environment with a fixed chemical potential.

2.1. *Basic theory; free energy and kinetic law*

One can assign free energy densities to the volume of bulk solid phases, the area of interfaces, and the length of triple junctions. Let g be the free energy per unit volume of atoms in a bulk solid phase (i.e. the chemical potential of the solid minus that of the vapor, divided by the atomic volume). In this paper we neglect the long range field and volume change associated with the phase change, and assume that g is uniform in each solid phase, but may differ in different phases. All solid phases are taken to have the same chemical composition. Let γ be the interfacial tension, which depends on the crystalline orientation of the interface. The free energy per unit length of a triple junction, Γ, may also affect the structural change when the grain size is extremely small. The total free energy of the system, G, has the three types of contributions:

$$G = \Sigma gV + \int \gamma \, dA + \int \Gamma \, dL. \tag{1}$$

The volume summation is over all solid phases, the surface integral over all interfaces, and the line integral over all triple junctions. The system of interfaces changes shape to reduce G.

Denote the free energy reduction per unit volume of atoms crossing an interface by p, to be called the driving pressure on the interface. By definition, p is not the pressure of a vapor on a solid surface. When a structure is not far from equilibrium, namely, when the free energy reduction per atom crossing an interface is small compared with the average thermal energy per atom, the normal velocity of the interface, v_n, is proportional to the driving pressure, p [6–8]. We adopt this kinetic law,

$$v_n = mp, \tag{2}$$

which defines the interface mobility m. Following Ref. [15], we express this theory into a form that suits finite element analysis. A system of interfaces with no triple junctions is considered first, followed by a discussion of the effect of triple junctions.

2.2. *Weak statement; a system of interfaces with no triple junction*

Figure 1 illustrates a single crystal particle immersed in a large mass of a vapor phase. The solid–vapor interface is a closed surface in three-dimensions. Imagine that the interface undergoes a virtual motion: each interface element moves in its normal direction as atoms are added to, or removed from, the solid; the magnitude of the interface displacement, δr_n, is infinitesimal and varies arbitrarily on the interface. The virtual motion need not obey any kinetic law. Associated with the virtual motion, the total free energy of the system varies by δG. Now define p more precisely as the total free energy reduction per unit interface area moving per unit distance, namely,

$$\int p \delta r_n \, dA = -\delta G. \tag{3}$$

The integral extends over the area of all interfaces.

When the interface tension is isotropic, p relates to the surface curvature by the Laplace–Young relation. Herring [5] derived expressions for p when the interface tension is anisotropic, and when the interface forms facets. The explicit expressions for p are unnecessary in formulating the finite element method, and will not be listed here.

Eliminating p in equation (3) by using the kinetic law (2), we have

$$\int \frac{v_n \delta r_n}{m} \, dA = -\delta G. \tag{4}$$

The actual velocity distribution, v_n, satisfies equation (4) for arbitrary distributions of the virtual motion, δr_n. We refer to this as the weak statement of the interface migration problem. This statement is the basis for the finite element method, as detailed in Section 3.

2.3. *Effect of triple junction*

Next consider a polycrystal, polyphase particle immersed in a large mass of a vapor. Various interfaces—phase and grain boundaries—intersect to form triple junctions. As before, δr_n is the virtual motion of an interface element, and p the associated force. The virtual motion of a line element of a triple junction, $\delta \mathbf{r}_t$, is a vector confined in the plane normal to the line element. Define the driving force for the

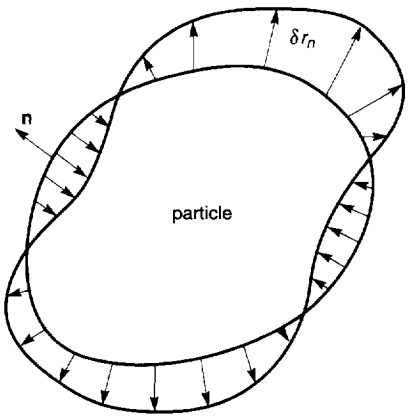

Fig. 1. A single crystal particle is immersed in a large mass of a vapor. The interface undergoes a distribution of virtual motion. The magnitude of the motion is infinitesimal, but is exaggerated in the figure.

junction motion, $\mathbf{f}_t$, as the free energy reduction per unit length moving per unit distance. Thus,

$$\int \mathbf{f}_t \cdot \delta \mathbf{r}_t \, dL + \int p \delta r_n \, dA = -\delta G. \tag{5}$$

Clearly, equation (5) is an extension of equation (3). (One could make a further extension to include the virtual motion of a grain corner.) Explicit expressions for $\mathbf{f}_t$ can be derived [15], but are unnecessary for formulating the finite element method.

We prescribe a kinetic law for the triple junctions:

$$\mathbf{v}_t = m_t \mathbf{f}_t. \tag{6}$$

Here $\mathbf{v}_t$ is the actual velocity, and m_t the mobility, of the triple junction.

Replacing the forces in equation (5) with the velocities using the kinetic laws (2) and (6), we obtain the weak statement involving both the interface and the junction motion:

$$\int \frac{\mathbf{v}_t \cdot \delta \mathbf{r}_t}{m_t} \, dL + \int \frac{v_n \delta r_n}{m} \, dA = -\delta G. \tag{7}$$

The actual velocities v_n and $\mathbf{v}_t$ satisfy equation (7) for arbitrary virtual motions δr_n and $\delta \mathbf{r}_t$.

2.4. *Equilibrium triple junction*

The triple junctions are commonly assumed to be in equilibrium at all times, even when the interfaces still move. At an equilibrated junction, the three interfaces meet at angles that balance the interface tensions. The assumption has been justified on the grounds that only a small number of atomic adjustments is needed for a junction to reach local equilibrium. The justification can be made definite as follows. Let d be a length scale to be resolved from a model, e.g. the depth of a surface groove. The effect of the junction mobility is negligible if $m_t d/m \gg 1$.

Assuming an equilibrium junction is equivalent to prescribing an infinitely large junction mobility: the first term in the weak statement (7) drops, which then becomes identical to equation (4). Consequently, the weak statement (4) determines interface velocities and equilibrates triple junctions simultaneously. In the finite element method based on the weak statement (4), we do not fix the interface angles. Rather, the equilibrium angles come out as a part of the solution in a short time. We will demonstrate this point with a numerical example.

3. DISCRETIZATION AND COMPUTATION

As stated above, the exact interface velocity satisfies the weak statement (4) for arbitrary virtual motions. The finite element method seeks an approximate interface velocity that satisfies equation (4) for a restricted family of virtual motions. An interface is modeled by an assembly of finite elements; the positions of nodes are the generalized coordinates. We now apply this method to a two-dimensional structure, where a grain is represented by an area, an interface by a curve, and a triple junction by a point.

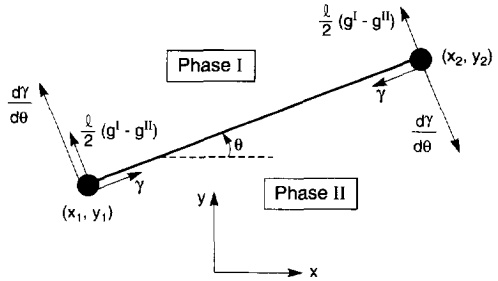

Fig. 2. A straight line element on an interface between phase I and II. When the element undergoes virtual motions, the free energy varies, exerting on the two nodes several forces: the axial force γ, the torque $d\gamma/d\theta$, and the lateral force $l(g^I - g^{II})/2$.

3.1. *Geometry of an element*

Following [14], we use an assembly of straight line elements to approximate an interface. Figure 2 shows one such element, on the interface separating phase I and II. The positions of the two nodes, (x_1, y_1) and (x_2, y_2), fully specify the geometry of the element. Denote the element length by l and the slope by θ; they relate to the nodal positions as $l \sin\theta = y_2 - y_1$ and $l \cos\theta = x_2 - x_1$. The virtual motion of the interface relates to the virtual motion of the nodal positions by

$$\delta r_n = N_1 \delta x_1 + N_2 \delta y_1 + N_3 \delta x_2 + N_4 \delta y_2, \tag{8}$$

with the interpolation coefficients being

$$N_1 = -\left(\tfrac{1}{2} - \frac{s}{l}\right)\sin\theta, \quad N_2 = \left(\tfrac{1}{2} - \frac{s}{l}\right)\cos\theta,$$

$$N_3 = -\left(\tfrac{1}{2} + \frac{s}{l}\right)\sin\theta, \quad N_4 = \left(\tfrac{1}{2} + \frac{s}{l}\right)\cos\theta.$$

Here, s is the distance measured on the element starting from the mid-point of the element. Similarly, the interface velocity relates to the nodal velocities, $\dot{x}_1$, $\dot{x}_2$, $\dot{y}_1$ and $\dot{y}_2$, by

$$v_n = N_1 \dot{x}_1 + N_2 \dot{y}_1 + N_3 \dot{x}_2 + N_4 \dot{y}_2. \tag{9}$$

3.2. *Forces acting on nodes by an element*

The surface tension depends on the crystalline orientation of the interface, as prescribed by a function $\gamma(\theta)$. For an interface modeled by straight line elements, γ is constant on each element, but takes different values on elements of different slopes. For a two-dimensional structure, the total free energy is

$$G = \Sigma \gamma(\theta) l + \Sigma g A. \tag{10}$$

The first summation is over the lengths of all the elements, and the second over areas of all the phases. The triple junctions become points in two dimensions, and have no free energy.

Associated with the virtual motion of a single element, the total free energy varies as

$$\delta G = \gamma \delta l + \frac{\mathrm{d}\gamma}{\mathrm{d}\theta} l \delta\theta - (g^{\mathrm{I}} - g^{\mathrm{II}}) l \frac{(\delta r_{\mathrm{n}})_1 + (\delta r_{\mathrm{n}})_2}{2}. \quad (11)$$

The first term is due to the elongation of the element; the second due to the rotation; and the third due to the trapezoidal area swept by the motion, where g^{I} and g^{II} are the free energy densities of the two bulk phases, and $(\delta r_{\mathrm{n}})_1$ and $(\delta r_{\mathrm{n}})_2$ are the virtual interface motions at the two nodes, directing from phase II to phase I. Figure 2 shows the physical significance of the forces acting on the nodes by the element. Each pair of forces is so directed to reduce the free energy.

Express the free energy variation in terms of virtual motions of the nodes:

$$\delta G = -f_1 \delta x_1 - f_2 \delta y_1 - f_3 \delta x_2 - f_4 \delta y_2. \quad (12)$$

Here f_i are the forces acting on the nodes by the element under consideration. Resolving the forces in Fig. 2 along the x and y directions, we obtain

$$\begin{bmatrix} f_1 \\ f_2 \\ f_3 \\ f_4 \end{bmatrix} = \gamma \begin{bmatrix} \cos\theta \\ \sin\theta \\ -\cos\theta \\ -\sin\theta \end{bmatrix} + \frac{\mathrm{d}\gamma}{\mathrm{d}\theta} \begin{bmatrix} -\sin\theta \\ \cos\theta \\ \sin\theta \\ -\cos\theta \end{bmatrix} + \frac{l(g^{\mathrm{I}} - g^{\mathrm{II}})}{2} \begin{bmatrix} -\sin\theta \\ \cos\theta \\ -\sin\theta \\ \cos\theta \end{bmatrix}. \quad (13)$$

3.3. *Virtual energy dissipation by an element*

The element also makes a contribution to the left-hand side of equation (4). The mobility m may also depend on the crystalline direction of the interface. For an interface modeled by straight line elements, m is constant on each element, but takes different values on elements of different slopes. Using equations (8) and (9), we have

$$\int \frac{v_{\mathrm{n}}}{m} \delta r_{\mathrm{n}} \, \mathrm{d}s = \{\delta x_1 \quad \delta y_1 \quad \delta x_2 \quad \delta y_2\} [H_{ij}] \begin{Bmatrix} \dot{x}_1 \\ \dot{y}_1 \\ \dot{x}_2 \\ \dot{y}_2 \end{Bmatrix}, \quad (14)$$

where $[H_{ij}]$ is a 4×4 symmetric matrix calculated from

$$H_{ij} = \frac{1}{m} \int_{-l/2}^{l/2} N_i N_j \, \mathrm{d}s, \quad (15)$$

giving

$$[H_{ij}] = \frac{l}{6m} \begin{bmatrix} 2\sin^2\theta & -2\sin\theta\cos\theta & \sin^2\theta & -\sin\theta\cos\theta \\ -2\sin\theta\cos\theta & 2\cos^2\theta & -\sin\theta\cos\theta & \cos^2\theta \\ \sin^2\theta & -\sin\theta\cos\theta & 2\sin^2\theta & -2\sin\theta\cos\theta \\ -\sin\theta\cos\theta & \cos^2\theta & -2\sin\theta\cos\theta & 2\cos^2\theta \end{bmatrix}. \quad (16)$$

3.4. *Assemble contributions from all elements*

Model a system of interfaces with n nodes. Assemble virtual changes of all the nodal positions to a column of dimension $2n$, $\delta\mathbf{x}$, and all the nodal velocities to another column, $\dot{\mathbf{x}}$. The weak statement (4) becomes

$$(\delta\mathbf{x})^{\mathrm{T}} \mathbf{H} \dot{\mathbf{x}} = (\delta\mathbf{x})^{\mathrm{T}} \mathbf{f}. \quad (17)$$

Here $\mathbf{H}$ is a matrix of dimension $2n \times 2n$, and $\mathbf{f}$ a column of dimension $2n$; both are assembled from the contributions from all the elements.

Since (17) holds for arbitrary virtual change $\delta\mathbf{x}$, it reduces to

$$\mathbf{H}\dot{x} = \mathbf{f}. \quad (18)$$

The matrix $\mathbf{H}$ relates the velocities to the forces; we will call it the viscosity matrix. It is a symmetric matrix as is evident from equation (15). Provided all nodal motions dissipate energy, the matrix is positive definite. Because the viscosity matrix and the force column depend on the nodal positions, equation (18) is a set of non-linear ordinary differential equations. For a given configuration of a structure, the viscosity matrix and the force column can be calculated, and equation (18) can be integrated for a time step. Repeat this procedure for many time steps to evolve the structure.

3.5. *Computational aspects*

A computer program is written to assemble the viscosity matrix and the force column, solve the velocities from equation (18) by Gaussian elimination, and update the nodal positions by the explicit fourth-order Runge–Kutta method. The program adapts time steps to limit the truncation error and nodal displacement increments. During a simulation, some elements shorten and others elongate. A very short element substantially reduces the time step; a very long element poorly models a curved geometry. We prescribe a minimum and a maximum element length. The program eliminates a very short element, and divides a very long one.

We have also encountered a problem specific to our discretization. When an interface tries to change the sign of curvature or to form a facet, a part of the interface becomes flat, with two or more elements aligning on the same straight line. The time step becomes exceedingly small, and the simulation often stops. The origin of this problem is as follows. A node on a flat interface may move either normal to the interface, or along the interface. The latter does not change the interface shape and has no physical significance. If the program follows the procedure blindly (and accurately), the viscosity matrix is

singular, and the force on the node vanishes, so that its velocity is undetermined. We have eliminated this problem by two approaches.

In the first approach, we assign large mobilities, m_x and m_y, at every node, similar to the triple junction mobility introduced above. The weak statement (4) is modified to be

$$\sum \frac{\dot{x}}{m_x}\delta x + \sum \frac{\dot{y}}{m_y}\delta y + \int \frac{v_n}{m}\delta r_n \, ds = -\delta G. \quad (19)$$

The first two terms sum over all nodes, and represent energy dissipation due to nodal motion. In the program, small positive numbers, $1/m_x$ and $1/m_y$, are added to the diagonal elements of the viscosity matrix to prevent it from becoming singular. Their exact values are unimportant, but should be large enough to remove the singularity in the viscosity matrix, and small enough not to disturb the system appreciably. We find that values of m/hm_x and m/hm_y between 10^{-6} and 10^{-3} are adequate, where m is the interface mobility and h a representative length of the system under study.

In the second approach, we use the normal interface displacement, δr_n, as the degree of freedom, and eliminate the tangential nodal motion from the calculation. This method has fewer degrees of freedom, but complicates the evaluation of the nodal forces. Triple junctions and facet corners have to be treated differently from the nodes in the middle of an interface.

For many crystals the function $\gamma(\theta)$ has cusps at certain values of θ corresponding to crystal planes of special orientations. These planes often have locally minimum surface tensions. At such a cusp (say at θ_1), $d\gamma/d\theta$ is discontinuous. Recall from Fig. 2 that $d\gamma/d\theta$ is the torque to rotate the element toward the orientation θ_1. Because $d\gamma/d\theta$ is discontinuous, an element slightly off the orientation θ_1 is subject to a large torque and therefore a large rotation velocity, which, in its turn, sets an exceedingly small time step, and vibrates the element near θ_1. This is a numerical artifact and nothing physically interesting happens. The element tries to do something very mundane: approach the equilibrium orientation corresponding to the low surface tension cusp. The numerical instability is avoided if the rotational degree of freedom is eliminated when an element is near a plane corresponding to a cusp. This approach would be similar to that of [10]. The problem is also avoided if the cusps in the $\gamma(\theta)$ function are excluded. For example, one may replace a cusp with a deep, but smooth valley. This latter approach modifies the physical problem, and should be used with caution. An example is given in the following section.

4. NUMERICAL EXAMPLES

This section gives examples solved with the finite element program. Some have analytical solutions that check the finite element program, others illustrate capabilities of the program. Similar programs have been developed to study grain growth [13, 14].

4.1. *Thermal grooving: isotropic surface tension*

When a polycrystalline particle is heated, the surface grooves along triple junctions to reduce the grain boundary area (with a small increase of the surface area). Mullins [7] gave an analytic solution to this problem, assuming that the particle surface is initially flat, and the surface energy γ_s and the grain boundary energy γ_b are isotropic. Figure 3(a) shows the initial geometry, consisting of a flat surface and a vertical grain boundary. The surface moves as atoms evaporate and condense. The free energy of the system increases by amount g when a unit volume of the solid phase condenses on a flat surface. When the groove depth d is so small that $gd/\gamma_b \ll 1$, the effect of g on grooving is negligible, and the grooving is driven mainly by γ_b and γ_s. Mullins assumed that $g = 0$, i.e. the vapor is in equilibrium with the flat solid surface far away from the grain boundary. Near the grain boundary, the surface evaporates at mobility m_s. Furthermore, when the groove depth is much smaller than the grain size, one can analyze the groove over a single grain boundary, and ignore all the other grain boundaries. The problem is two dimensional.

Figure 3(b) indicates two angles at the triple junction, the dihedral angle Ψ, and the surface slope θ_0; they are related as $\Psi + 2\theta_0 = \pi$. The angles are determined by the balance law of surface tensions, e.g.

$$\sin\theta_0 = \frac{\gamma_b}{2\gamma_s}. \quad (20)$$

According to the local equilibrium assumption, this angle is maintained at all times, including $t = 0$.

The initial geometry does not have any length scale, but the dynamical system does have a length

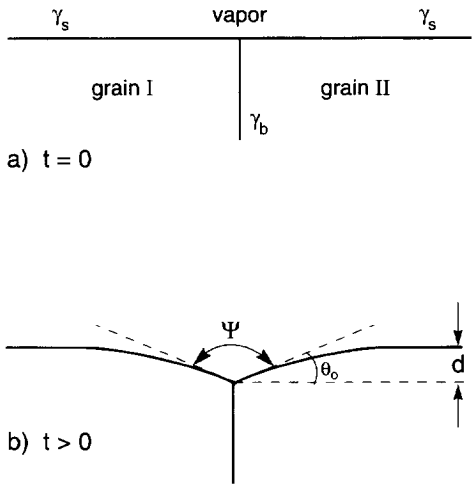

Fig. 3. A triple junction of a grain boundary and a solid–vapor interface. (a) At $t = 0$, the interface is flat. (b) As the time proceeds, the interface grooves when atoms evaporate.

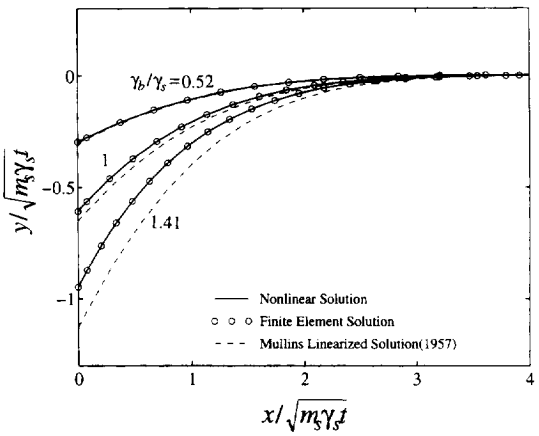

Fig. 4. A comparison of groove profiles solved by several methods. The surface tension is isotropic.

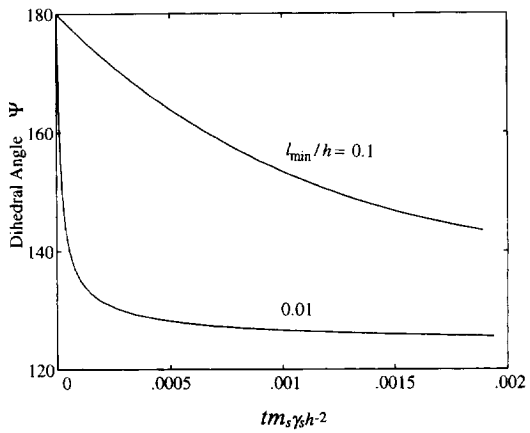

Fig. 5. In the finite element analysis, the dihedral angle approaches its equilibrium value in finite time, dictated by element size.

scale, $(m_s\gamma_s t)^{1/2}$. As the time t increases, the groove profile is self-similar and scales with this length; for example, the groove depth d indicated in Fig. 3(b) is proportional to this length scale. Mullins further assumed that γ_b/γ_s is small, so that the slope of the surface is small everywhere. Under this assumption, the differential equation that governs the surface evolution can be linearized, and the groove depth is linear in $\tan\theta_0$, which enters the problem as a boundary condition. His solution gives

$$d \approx 1.13 \tan\theta_0 (m_s\gamma_s t)^{1/2}. \tag{21}$$

The surface profile obtained by Mullins is plotted in Fig. 4. Also included for comparison are the solutions to the non-linear ordinary differential equation for the self-similar profile (see [15]).

The same problem is now analyzed using the finite element program. The surface of one grain is modeled with about 40 elements. The grain boundary does not migrate; it enters the problem by applying a force γ_b at the triple junction. Figure 4 plots the profiles of the surface calculated from the finite element program. They agree with the solutions to the non-linear ordinary differential equation.

In the finite element analysis, a perfectly flat surface is assumed at $t = 0$. The equilibrium dihedral angle is not prescribed, but comes out as part of a solution in a short time. The time needed for the dihedral angle to reach equilibrium depends on the element size near the triple junction: the smaller the elements, the shorter the time. Figure 5 shows, with two element lengths, the calculated dihedral angle Ψ as a function of time for the system with $\gamma_b = \gamma_s$. An arbitrary length h is used in normalizing the element length and the time. The dihedral angle is off the equilibrium value $\Psi = 120^\circ$ initially, but approaches the equilibrium value. Suppose one is interested in resolving a length scale from the calculation, e.g. the groove depth at some finite time. Provided the element size is smaller than the length scale to be resolved, the non-equilibrium triple junction during a short time in the beginning does not affect the result appreciably, as confirmed in Fig. 4 by the comparison with the solutions obtained by other methods.

4.2. *Thermal grooving: finite junction mobility*

In the preceding example, the junction mobility is taken to be so large that it quickly equilibrates. We now examine the effect of a finite junction mobility on surface grooving. The configuration still starts with a flat surface and a vertical grain boundary in Fig. 3(a). The surface mobility is m_s and the junction mobility m_t. The problem has only two-dimensionless parameters: γ_b/γ_s and $t\gamma_s m_t^2/m_s$. The profile is no longer self-similar. For small γ_b/γ_s, the slope of the surface at the triple junction is linear in γ_b/γ_s. Extending equation (20) we write

$$\sin\theta_0 \approx \frac{\gamma_b}{2\gamma_s} F\left(\frac{t\gamma_s m_t^2}{m_s}\right). \tag{22}$$

Figure 6 plots the function F computed by the finite element method. Everything else being fixed, $\sin\theta_0$

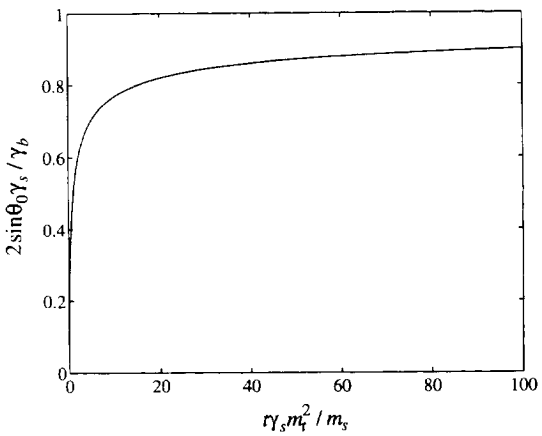

Fig. 6. The effect of junction mobility on the surface slope at the triple junction.

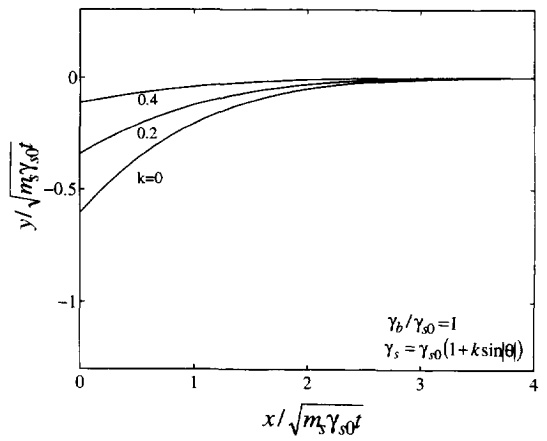

Fig. 7. Groove profiles determined by finite element analysis. The surface tension is anisotropic.

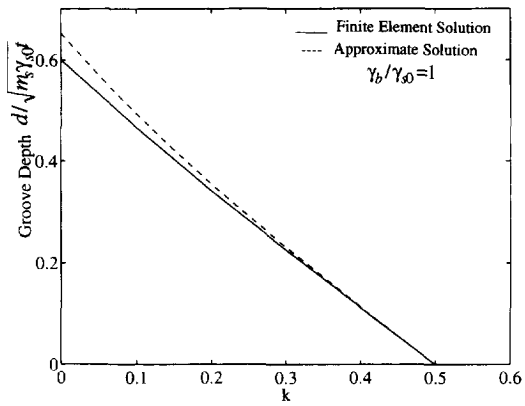

Fig. 8. The groove depth as a function of the anisotropic coefficient k.

starts at zero, increases with the time, and approaches the equilibrium value $\gamma_b/2\gamma_s$. The time needed to attain the equilibrium angle scales with $m_s/(m_i^2\gamma_s)$.

4.3. *Thermal grooving: anisotropic surface tension*

We next study the effect of surface tension anisotropy on grooving. Assume that the surfaces of the two grains in Fig. 3 are crystallographically equivalent, and have the same surface tension function $\gamma_s(\theta)$, where θ is the slope of the surfaces. Further assume that $\gamma_s(\theta)$ is an even function, with a minimum at $\theta = 0$. Because the slope of the surface is typically small, we only need to prescribe $\gamma_s(\theta)$ in the vicinity of $\theta = 0$. The following function is adopted in the calculation:

$$\gamma_s(\theta) = \gamma_{s0}(1 + k \sin|\theta|), \tag{23}$$

with $k > 0$. The function has a cusp at $\theta = 0$.

The local equilibrium assumption requires that the slope of the surface at the triple junction, θ_0, be solved from [5]

$$2\gamma_s \sin\theta_0 + 2\cos\theta_0 \frac{d\gamma_s}{d\theta} = \gamma_b. \tag{24}$$

Inserting (23) into (24), we find the surface slope at the triple junction:

$$\sin\theta_0 = \frac{\gamma_b}{2\gamma_{s0}} - k. \tag{25}$$

The horizontal surface has the lowest surface tension, so that the surface tension anisotropy reduces the surface slope.

The surface mobility m_s is taken to be isotropic. The surface profile is still self-similar, all the lengths scaling with $(m_s\gamma_{s0}t)^{1/2}$. Figure 7 shows the surface profiles calculated using the finite element program. The calculated slopes of the surface at the triple junction agree well with equation (25). The groove depth d is proportional to $(m_s\gamma_{s0}t)^{1/2}$ and, under the small slope assumption, is linear in $\tan\theta_0$. Equation (21) suggests a similar approximation:

$$d \approx 1.13 \tan\theta_0 (m_s\gamma_{s0}t)^{1/2}. \tag{26}$$

Now θ_0 is given by equation (25). This approximation is compared with the finite element solutions in Fig. 8 for the case $\gamma_b/\gamma_{s0} = 1$. The approximation is better for smaller values of γ_b/γ_{s0}.

4.4. *Competition of grain boundary motion and thermal grooving in thin film*

In a previous paper [16], we have studied competitive motion of grain boundaries and free surfaces in a thin film. Fast grain boundary motion results in a film with large grains. Fast surface motion causes grooves along the triple junctions and breaks the film to islands. One such calculation is extended here. At the beginning of the calculation, the film has a flat free surface and a vertical grain boundary (Fig. 9(a)). For all three calculations described below, various interface tensions are indicated in the figure

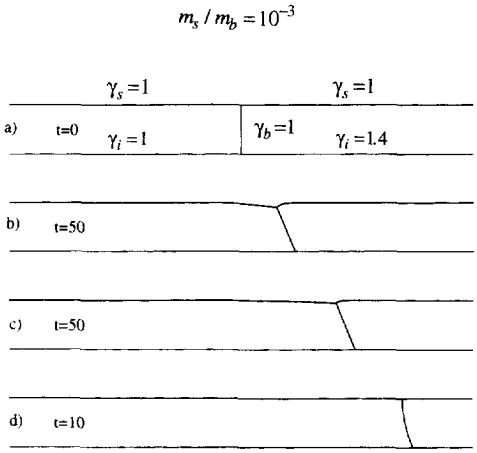

Fig. 9. (a) Initial configuration of a two-grain thin film on a substrate. (b) The grain boundary is pinned by the groove. (c) Finite junction mobility delays the groove development, allowing the grain boundary to move a longer distance. (d) Surface tension anisotropy modifies groove angle significantly, so that the grain boundary moves very fast.

in units of γ_b, the film–substrate interface is immobile, and the film surface has a low mobility compared with the grain boundary mobility, $m_s/m_b = 10^{-3}$. The time indicated in each subsequent figure is normalized by $h^2/\gamma_b m_b$, where h is the film thickness.

Figure 9(b) assumes that the surface tension is isotropic, and the junction mobility is very large. The grain boundary is pulled by the difference in the film–substrate interface tensions, but is pinned by its triple junction with the film surface. The grain boundary becomes nearly straight, and migrates very slowly. The groove will eventually grow through film thickness.

Figure 9(c) shows the effect of a finite junction mobility, $hm_t/m_b = 10^{-2}$. As discussed before, with a finite junction mobility, the triple junction needs a finite time to approach to its equilibrium value. Consequently, the grain boundary can migrate over a longer distance than that in Fig. 9(b) in the same time period. The triple junction will eventually groove down to the substrate.

Figure 9(d) shows the effect of surface tension anisotropy. The surface tension of the film surface varies with the slope according to equation (23), with $\gamma_{s0}/\gamma_b = 1$ and $k = 0.3$. The anisotropy changes the surface angles at the junction, so that the grain boundary is no longer pinned by the groove and moves very fast. Clearly, surface tension anisotropy plays a decisive role in thin film morphology selection.

4.5. *Facet formation*

Due to surface tension anisotropy, small particles of many crystals take shapes of polyhedrons, with flat facets and sharp edges and corners. Given the surface tension as a function of the crystal surface normal, the Wullf construction determines the shape of the crystal particle that minimizes the total surface energy. A particle in reality may differ from the Wullf shape for many reasons. It may be too large to have equilibrated. It may contain a defect like a twin boundary that modifies energetics. We now give a simple example to demonstrate the capability of the program to evolve a crystal that forms facets. In the calculation, the surface tension has a four-fold symmetry, having a form

$$\gamma(\theta) = \gamma_0(1 - b\cos 4\theta), \tag{27}$$

with $b = 0.3$. To avoid the numerical problem discussed at the end of Section 3, we have chosen this function with smooth valleys.

An initially circular particle of radius R_0 is immersed in a large mass of its vapor ($g = 0$). The particle simultaneously changes shape and loses mass to the vapor. The surface mobility, m_s, is assumed to be isotropic. Figure 10 shows three snapshots of the evolution. The time is reported in unit $R_0^3/m_s\gamma_0$. Immediately after the simulation begins, the surface forms small facets, the length of the facets being limited by the element size. The facets then grow in size and reduce in number ($t = 0.1$). At some time ($t = 0.3$), only four facets remain, as dictated by the Wullf construction. Because the function (27) has smooth valleys rather than cusps, the facets are not perfectly flat. The particle reduces its size with the self-similar shape afterwards.

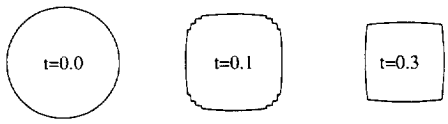

Fig. 10. A circular particle forms facets due to surface tension anisotropy.

5. CONCLUDING REMARKS

During fabrication, a material selects its microstructure by a dynamical process, rather than an equilibrium state. Structural entities co-evolve under multiple forces via concomitant rate processes. The complexity underlies industrial innovations and calls for robust simulation tools. The finite element method for simulating interface migration has several advantages. It handles isotropic and anisotropic surface tension in a unified way. Triple junctions equilibrate automatically, or can be controlled independently. A preliminary survey [15] has indicated that other kinetic processes, such as diffusion on interfaces and creep in grains, can be included in the same framework, so can long range elastic and electric fields. Building on the mature knowledge base of finite element codes for stress analysis, a code for interface motion would be a robust tool to evolve complex structures, and have the option to link to the stress analysis codes.

Acknowledgements—The work was supported by NSF through grant MSS-9258115, and by ARPA through a URI contract N-0014-92-J-1808. Yang was supported by a visiting appointment at the University of California, Santa Barbara, partly funded by ONR through contract N00014-93-1-0110.

REFERENCES

1. M. A. Spears and A. G. Evans. *Acta metall.* **30,** 1281 (1982).
2. F. F. Lange, *J. Am. Ceram. Soc.* **72,** 3 (1989).
3. C. V. Thompson, J. Floro and H. I. Smith, *J. appl. Phys.* **67,** 4099 (1990).
4. D. J. Srolovitz and S. A. Safran, *J. appl. Phys.* **60,** 247 (1986).
5. C. Herring, in *The Physics of Powder Metallurgy* pp. 143–179 (edited by Kingston). McGraw-Hill, New York (1951).
6. D. Turnbull, *Solid State Physics* **3,** 225 (1956).
7. W. W. Mullins, *J. appl. Phys.* **28,** 333 (1957).
8. W. W. Mullins, *J. appl. Phys.* **27,** 900 (1956).
9. H. J. Frost, C. V. Thompson and D. T. Walton, *Acta metall. mater.* **40,** 779 (1992).
10. W. C. Carter, A. R. Roosen, J. W. Cahn and J. E. Taylor, *Acta metall. mater.* **43,** 4309 (1995).
11. B. Sun, Z. Suo and A. G. Evans, *J. Mech. Phys. Solids* **42,** 1653 (1994).

12. R. Loge and Z. Suo, *Acta mater.* **44,** 3429–3438 (1996).
13. A. C. F. Cocks, and S. P. A. Gill, *Acta mater.* **44,** 4765 (1996).
14. Z. Z. Du, R. M. McMeeking, and A. C. F. Cocks, manuscript in preparation.
15. Z. Suo, *Advances in Applied Mechanics* **33** (1996).
16. B. Sun, Z. Suo and W. Yang, Competitive motions of grain-boundary and free surface in selecting thin film morphology. *Mater. Res. Soc. Symp. Proc.*, in press.